Multifunctional 3D-printed patches for long-term drug release therapies after myocardial infarction

Ajdary, Rubina

2020-08-19

Ajdary , R , Zanjanizadeh Ezazi , N , Rebelo Correia , A M , Kemell , M , Huan , S , Ruskoaho , H , Hirvonen , J , Santos , H A & Rojas , O J 2020 , ' Multifunctional 3D-printed patches for long-term drug release therapies after myocardial infarction ' , Advanced Functional Materials , vol. 30 , no. 34 , 2003440 . https://doi.org/10.1002/adfm.202003440

http://hdl.handle.net/10138/318423
https://doi.org/10.1002/adfm.202003440

ADVANCED FUNCTIONAL MATERIALS
www.afm-journal.de

Multifunctional 3D-Printed Patches for Long-Term Drug Release Therapies after Myocardial Infarction

Rubina Ajdary, Nazanin Zanjanizadeh Ezazi, Alexandra Correia, Marianna Kemell, Siqi Huan, Heikki J. Ruskoaho, Jouni Hirvonen, Hélder A. Santos, and Orlando J. Rojas**

A biomaterial system incorporating nanocellulose, poly(glycerol sebacate), and polypyrrole is introduced for the treatment of myocardial infarction. Direct ink writing of the multicomponent aqueous suspensions allows multifunctional lattice structures that not only feature elasticity and electrical conductivity but enable cell growth. They are proposed as cardiac patches given their biocompatibility with H9c2 cardiomyoblasts, which attach extensively at the microstructural level, and induce their proliferation for 28 days. Two model drugs (3i-1000 and curcumin) are investigated for their integration in the patches, either by loading in the precursor suspension used for extrusion or by direct impregnation of the as-obtained, dry lattice. In studies of drug release conducted for five months, a slow in vitro degradation of the cardiac patches is observed, which prevents drug burst release and indicates their suitability for long-term therapy. The combination of biocompatibility, biodegradability, mechanical strength, flexibility, and electrical conductivity fulfills the requirement of the highly dynamic and functional electroresponsive cardiac tissue. Overall, the proposed cardiac patches are viable alternatives for the regeneration of myocardium after infarction through the effective integration of cardiac cells with the biomaterial.

1. Introduction

Nanofibrillated cellulose (CNF) has emerged as a promising nanostructured material exhibiting versatile properties for a wide range of applications, in particular in the biomedical fields.[1,2] Nanocellulose has similarities with the extracellular matrix (ECMs), it is biocompatible and can be assembled in highly porous structures.[3] Aqueous suspensions of nanocellulose are shear-thinning, which facilitate extrusion via direct ink writing (DIW),[4–6] which has been used to develop highly porous (99.7%) and swellable (447 g water g^{-1}) scaffolds.[7] Moreover, they have been proven to be nontoxic, highly stable and compatible with fibroblast,[4] H9c2 cardiac myoblast,[3] and Murine preosteoblastic (MC3T3-E1) cells.[8] Notably, to fully exploit the properties of scaffolds based on nanocellulose, consideration should be given to the processing technique. In this respect, several approaches have been introduced, including gel casting,[9] electrospinning,[10] and 3D printing.[4] The latter approach is particularly useful to gain control on the morphological organization of the scaffold, including its geometry, gradient porosity, and pore orientation, and also to achieve tunable mechanical properties.[11,12]

Although 3D printing has opened new avenues for the development of tailorable structures, several challenges still remain. They include the need to optimize the composition to achieve 3D-printable inks, the high water content of the

R. Ajdary, Prof. O. J. Rojas
Department of Bioproducts and Biosystems
School of Chemical Engineering
Aalto University
P.O. Box 16300, Aalto, Espoo FI-00076, Finland
E-mail: orlando.rojas@aalto.fi

N. Z. Ezazi, A. Correia, Prof. J. Hirvonen, Prof. H. A. Santos
Drug Research Program
Division of Pharmaceutical Chemistry and Technology
Faculty of Pharmacy
University of Helsinki
Helsinki FI-00014, Finland
E-mail: helder.santos@helsinki.fi

The ORCID identification number(s) for the author(s) of this article can be found under https://doi.org/10.1002/adfm.202003440.

DOI: 10.1002/adfm.202003440

Dr. M. Kemell
Department of Chemistry
University of Helsinki
Helsinki FI-00014, Finland

Dr. S. Huan, Prof. O. J. Rojas
Bioproducts Institute
Departments of Chemical & Biological Engineering
Chemistry and, Wood Science
2360 East Mall, The University of British Columbia, Vancouver, BC V6T 1Z3, Canada

Prof. H. J. Ruskoaho
Drug Research Program
Division of Pharmacology and Pharmacotherapy
University of Helsinki
Helsinki FI-00014, Finland

Prof. H. A. Santos
Helsinki Institute of Life Science (HiLIFE)
University of Helsinki
Helsinki FI-00014, Finland

respective gels and the extensive shrinkage of the obtained structures upon removal of the water.[13] The potential of nanocellulose as a highly stable, 3D printed material has been demonstrated for cell culturing scaffolds;[3] however, such structures lack some critical properties such as elasticity. Thus, additional components are required to enhance, tune, or facilitate given properties in the nanocomposite and to match the targeted application. Here, poly(glycerol sebacate) (PGS), a biodegradable and cost-effective polymer commonly used in biomedical devices, was combined with nanocellulose to alter its mechanical behavior, particularly to enable scaffolds with elasticity and flexibility. The application of PGS targets the soft tissue along with tailorable mechanical properties as defined by the synthesis method.[14–16] Importantly, in a recent study,[17] we reported cardiac patches based on PGS loaded with polypyrrole (PPy), a heterocyclic conductive polymer,[17,18] which facilitated both cytocompatibility and electrical conductivity.[19–21]

As a new development of this earlier work, we propose the incorporation of nanocellulose not only to facilitate direct ink writing but to act as active component in the scaffolds used as cardiac patches. Such materials are of high interest in the treatment of cardiovascular diseases, which according to the World Health Organization (WHO), represent the principal cause of deaths worldwide (31% of the total), amounting to 17.9 million patients per year.[22] As the adult human hearts possess a negligible regenerative capacity, cardiomyocyte loss in response to myocardial infarction leads to scar formation, remodeling of the surrounding myocardium, progressive impairment of cardiac function, and eventually to heart failure.[23] Solutions, such as cell-based therapy and organ transplantation have been implemented;[24–27] however, they are often associated with complications, such as deficient cell injection, immune rejection, and insufficient nutrition supply.[19,28,29]

These limitations have encouraged the development of alternative approaches to regenerate the infarcted heart tissue, for example, through the integration of cardiac cells and biomaterials.[28] Related biomaterials can perform as mechanical support for cells and promote their reorganization into a functional tissue.[30] Thus, there is a demand for scaffolds that are similar to the ECM and mimic the original tissue, e.g., by holding cardiomyocytes and other cardiac cells, while facilitating myocardial regeneration.[31,32] In addition to biocompatibility and biodegradability, such cardiac scaffolds should fulfill several other properties, including mechanical strength and electrical conductivity, so that the dynamic functions of electroresponsive cardiac tissue are maintained.[17,33]

The materials used for cardiac tissue engineering can be of natural origin (such as gelatin,[29,33,34] alginate,[35,36] chitosan,[32] collagen,[17,35] bacterial nanocellulose,[37] and fibrin),[38] synthetic (including polyurethane,[39,40] polycaprolactone,[40] poly(lactic acid),[41,42] poly(glycolic acid)),[42] as well as composite and hybrid materials,[17] which combine natural, synthetic or metallic compositions.[43,44] In the first category, some biopolymers have the advantage of being similar to the ECM; however, the balance between swelling stability and mechanical strength remains challenging.[45]

According to previous studies, crosslinking or addition of complexing agents enhances the mechanical strength of natural polymers, as well as their stability in the given scaffold.[46,47] Unfortunately, the most widely used crosslinkers in biomedical applications, namely, glutaraldehyde and genipin, are cytotoxic and the removal of unreacted molecules become a necessity to facilitate cell growth.[48] Overall, we study 3D-printed cardiac patches based on nanocellulose, PGS and PPy, which were tested for load and release of two model drugs. The drug selection was in accordance with the antioxidant and anti-inflammatory activity (curcumin),[49,50] as well as the efficacy in promoting myocardial repair after myocardial infarction and other injuries (3i-1000).[17,51–53] These drugs were loaded in the ink before 3D printing (ink-loaded) and also by immersion in the drug solution of the ready-made patches (immersion-loaded). In addition, the two methods were tested by sequentially applying ink-loading and immersion-loading (referred to as ink-immersion loading). The release profiles of these systems were monitored for five months. This work follows our recent efforts confirming the biocompatibility of H9c2 cardiomyoblast with highly stable nanocellulose scaffolds,[3] as well as the promising results related to H9c2 cardiomyoblast–biomaterial interactions in PGS-collagen-PPy 2D-casted films.[17] Thus, we introduce a suitable composition in the form of 3D-printed cardiac patches based on plant-based nanocellulose that fulfills requirements such as biocompatibility, elasticity, and electrical conductivity, comparable to those of native cardiac tissue.[54] The morphology, microstructure, and porosity of the biocomposites were examined and the biological responses evaluated through cell viability, proliferation, and attachment.

2. Results and Discussion

2.1. Elastic and Conductive Nanocellulose-Based Composite Patches

2.1.1. Ink Composition

Several compositions of 2,2,6,6-tetramethylpiperidine-1-oxyl radical-oxidized nanocellulose (TOCNF), pre-PGS, and PPy were tested to provide a suitable shear flow behavior and to endow the printed patches with mechanical integrity and electrical conductivity. As indicated in **Figure 1**a, TOCNF was used as principal component and support phase for pre-PGS and PPy, which were added to provide elasticity and conductivity. According to differential scanning calorimetry, no thermal degradation occurred for neat TOCNF or sample 5% 1:2 at the processing temperature (Figure S1, Supporting Information). All inks were shear thinning, with a dominant elastic behavior (Figure S2, Supporting Information). The 3D-printed patches contained over 95% solvent, leading to an extensive shrinkage upon drying. To limit such effect, the samples were freeze-dried, resulting in the preservation of the structure and its porosity, prior to the curing of pre-PGS in vacuum oven at 120 °C for 48 h. The patches underwent ≈5% and 14% shrinkage after freeze-drying followed by pre-PGS curing (vacuum oven), respectively (Figure 1b–d).

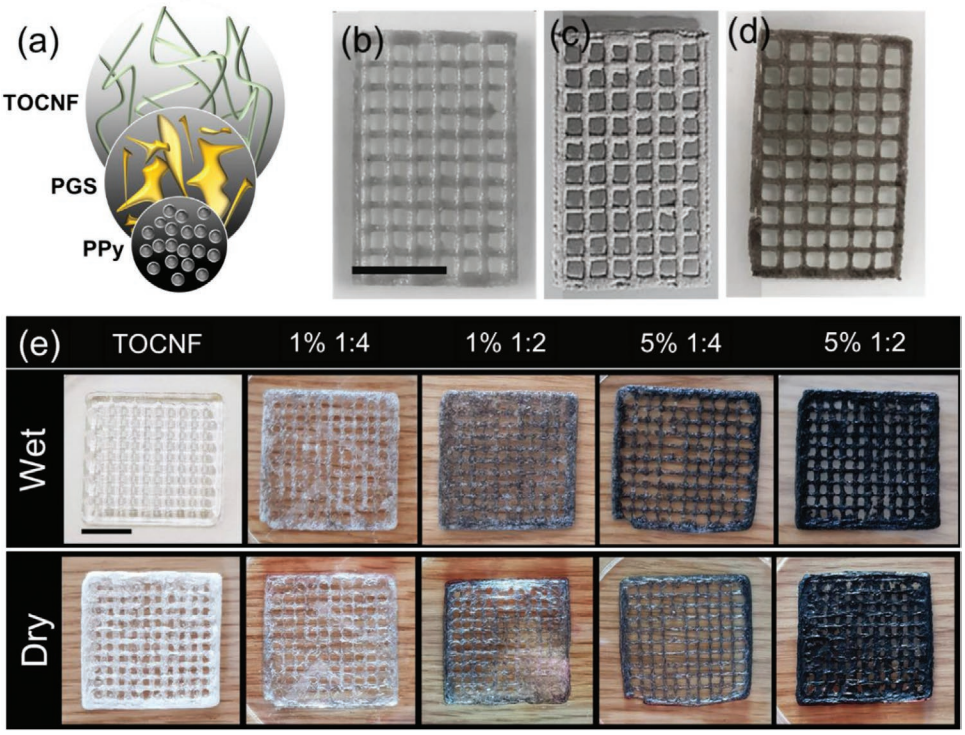

Figure 1. a) Schematic illustration (not to scale) of TOCNF, pre-PGS, and PPy used in the formulation of DIW inks and 3D-printed scaffolds b) before and c) after freeze-drying. d) Scaffold after pre-PGS curing for 48 h at 120 °C. e) 3D printed samples of given component ratio, wet and cured (the % figure corresponds to PPy % and the ratio refers to the relative volume of pre-PGS-PPy to weight of TOCNF). The scale bar in (b)–(e) corresponds to 1 cm.

2.2. 3D-Printed Patches

2.2.1. Patch Morphology

Transmission electron microscopy (TEM) revealed the typical morphology of the cellulose nanofibrils (TOCNF), displaying a high axial aspect, **Figure 2** (left). The biocomposite systems used for 3D printing included the negatively charged nanocellulose and the cationic mixture consisting of pre-PGS and PPy, which formed interfacial electrostatic complexes (shown in Figure 2 (right) is the system labeled as "5% 1:2" (PPy w/v%, PGS-PPy:TOCNF), see legend of Figure 1 for nomenclature).[21][55] After curing at high temperature and under vacuum, the PGS component endows the TOCNF-based system with elasticity.

2.2.2. Microstructure and Porosity

The nanocellulose-based scaffolds displayed interconnected pores that are expected to facilitate a suitable environment for cells to grow and interact (**Figure 3**a).[3] Single component

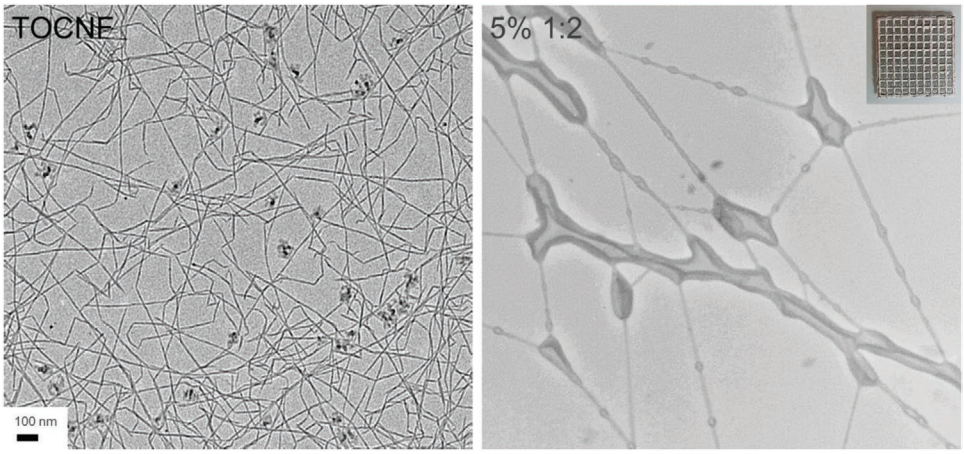

Figure 2. TEM images of the samples comprising a) neat TOCNF and b) 3D printed TOCNF composite with PGS and PPy after curing (5% 1:2 system according to the nomenclature presented in the legend of **Figure 1**). The scale bar corresponds to 100 nm.

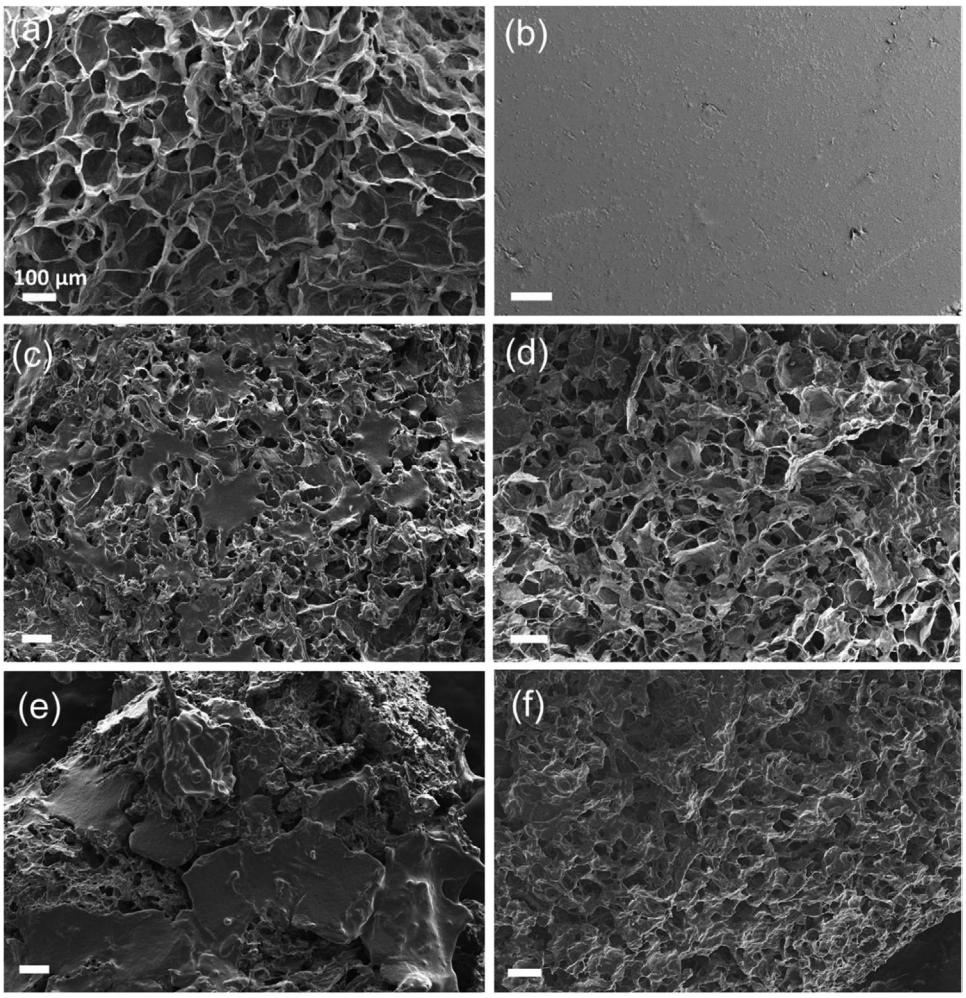

Figure 3. Scanning electron microscope (SEM) images of patches produced with a) neat TOCNF; b) casted and cured PGS-PPy 5%; c) 5% 1:4 and e) 5% 1:2 before PGS synthesis, showing phase separation of TOCNF and pre-PGS. d) 5% 1:4 and f) 5% 1:2 after pre-PGS curing, illustrating the formation of PGS-PPy-TOCNF biocomposite. The scale bars correspond to 100 µm.

TOCNF scaffolds (Figure 3a), were remarkably more porous (94 ± 1% porosity) compared to those produced with PGS-PPy (Figure 3b) or with the multicomponent counterparts. Overall, TOCNF enhances the porosity and permeability of the structure, which are factors that favor cells attachment.[3] Figure 3c–f compares microstructures obtained before and after PGS synthesis. Phase separation of TOCNF and pre-PGS-PPy is evident, Figure 3c,e. After pre-PGS curing, the phases formed a homogenous biocomposite structure with 78 ± 2% porosity.

2.2.3. Electrical Conductivity and Mechanical Properties

Systems containing 1% PPy were not electrically conductive; therefore, we focus the discussion on samples with a higher PPy loading, which were electrically conductive. We note that a high nanocellulose loading produced patches with an uneven conductivity, as measured in different areas of the structure, which is explained by the pores generated upon removal of water, as expected.[56] As shown in **Table 1**, The 5% 1:2 system presented an electrical conductivity of 34 mS cm^{-1}. This value is relatively lower than those measured for nanocellulose-PPy composites previously prepared from precursors such as hydrogels, sponges, and coatings (electrical conductivity in the range of ≈80–150 mS cm^{-1}), suitable for paper-based energy storage devices and composites for nerve regeneration.[57–59] However, for the present purpose, the produced patches were determined to have a suitable conductivity.

Turning our attention to the mechanical strength of the patches, we note that the elastic modulus of human myocardium ranges from 0.02 to 0.5 MPa,[15] while the values for pure PGS varies between 0.056 and 1.5 MPa, depending on

Table 1. Main characteristics of patches of given composition.

Sample	Electrical conductivity [mS cm^{-1}]	Young's modulus [MPa]	Elongation [%]	Porosity [%]
TOCNF	0	0.2 ± 0.04	2	94 ± 1
5% 1:4	3 ± 1.3	–[a)]	–	–
5% 1:2	34 ± 2.7	0.6 ± 0.16	18	78 ± 2

[a)] "–": Not available.

the curing time.[60] The Young's modulus of the biocomposites increased considerably (three-fold) upon addition of TOCNF, reaching a value comparable with that of the human myocardium. Compared to pure PGS, the presence of nanocellulose limits the elongation of the composite; however, the measured value still meets the performance criteria, as indicated in previous reports.[61,62] Moreover, compared to the porosity of patches formed from neat TOCNF, the values corresponding to systems containing PGS and PPy decreased by ≈17%. However, this reduction in porosity did not have a significant impact on cell–biocomposite interactions, as discussed in later sections.

2.2.4. Degradation and Swelling of 3D Printed Scaffolds

The structural stability, extent of biomaterial degradation and its rate are essential factors for drug administration.[63] As such, patch swelling (absorption capacity) and degradation rate in aqueous media were examined during 21 days using buffered media at two pH values. Degradation in MES (pH 6) was faster compared to that in Phosphate-buffered saline (pH 7.4), which occurred only after 14 days, **Figure 4**a. In general, the presence of TOCNF did not significantly affect the degradation in 2-(N-morpholino)ethanesulfonic acid buffer, but a higher degradation in PBS (pH 7.4) was observed at low TOCNF loading. Despite the absence of crosslinker, the 3D biocomposites were strongly networked and showed 6–7% degradation based on the initial mass. According to previous studies, highly crystalline cellulose structures prevent degradation, which would otherwise occur by enzymatic activity or a combination of autocatalytic oxidation and hydrolytic mechanisms.[64,65] As shown in our previous research, the addition of PPy does not affect the degradation rate;[17] therefore the degradation mostly involved the PGS component.[66]

Figure 4b shows the swelling of the patches, which indicated >200% water absorption with respect to the initial mass, highlighting the contribution of TOCNF (systems with cellulose nanofibrils alone absorbs more than 1000% its dry mass) (Figure S3, Supporting Information).[3] Owing to the carboxylic groups present in TOCNF, an extensive swelling in MES was observed at high TOCNF loadings (days 1, 14). Swelling is an essential factor as it relates to the ability to absorb the fluid medium after implantation, which facilitates nutrient and oxygen transport inside the system, as well as cell infiltration.[18] In the medium, the patch must be stable even in the swollen state. In the present system, owing to the presence of highly stable TOCNF, the patches underwent swelling while maintaining microstructural integrity.

2.2.5. Cell Viability, Proliferation, and Attachment of the 3D Printed Scaffolds

The biocompatibility of 3D printed composites undergoing degradation was examined by using the 3-(4,5-dimethylthiazol-2-yl)-2,5-diphenyltetrazolium Bromide (MTT) assay and compared with a positive control (empty incubated medium). As shown in **Figure 5**a, the degradation of the different patches did not affect the viability of H9c2 cardiomyoblast. No cytotoxicity was detected during 28 days; even at day one, a slight proliferation was observed for cells in the vicinity of the degraded biocomposites.

As illustrated in Figure 5b, all types of 3D printed biocomposites showed an ability to host cardiomyoblasts for proliferation. No significant differences were observed in H9c2 cell proliferation for patches at the different PPy loadings. We reported cell proliferation and attachment of cells on TOCNF[3] and PGS-collagen-PPy 2D heart patches.[17] Here, TOCNF was freeze-dried and placed in a vacuum oven at 120 °C under low pressure, e.g., to maintain the same conditions as those used in the synthesis of the biocomposites. The standard deviation shows that the proliferation of the H9c2 cells on 3D-printed composites were in the same range as that for the TOCNF porous structure. The cells proliferated around twice in each two weeks. This result points to the capability of the scaffolds to both, host the cells and to create a suitable environment for proliferation. Cell–biocomposite interactions for 4 days indicated that the patches, with their porous structures (scanning electron microscopy, SEM), allowed good attachment. Cell bodies assembled on the pore surface and elongated on the pore walls with high extension and adhesion. Figure 5c,d illustrates the empty control sample and the cell-seeded biocomposite, respectively. The results confirm the cell viability tests and show a positive interaction between H9c2 cardiomyoblast and the 3D-printed, conductive patch following cell infiltration. The TOCNF and PGS hydrophilicity, high porosity, and surface area make the system suitable for cell attachment while remaining viable.

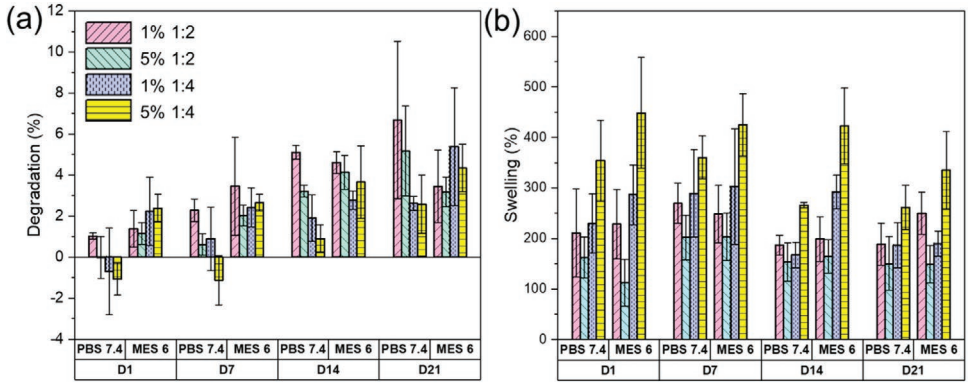

Figure 4. a) Degradation and b) swelling of 3D-printed cardiac patches measured in PBS (pH 7.4) and MES (pH 6) buffers.

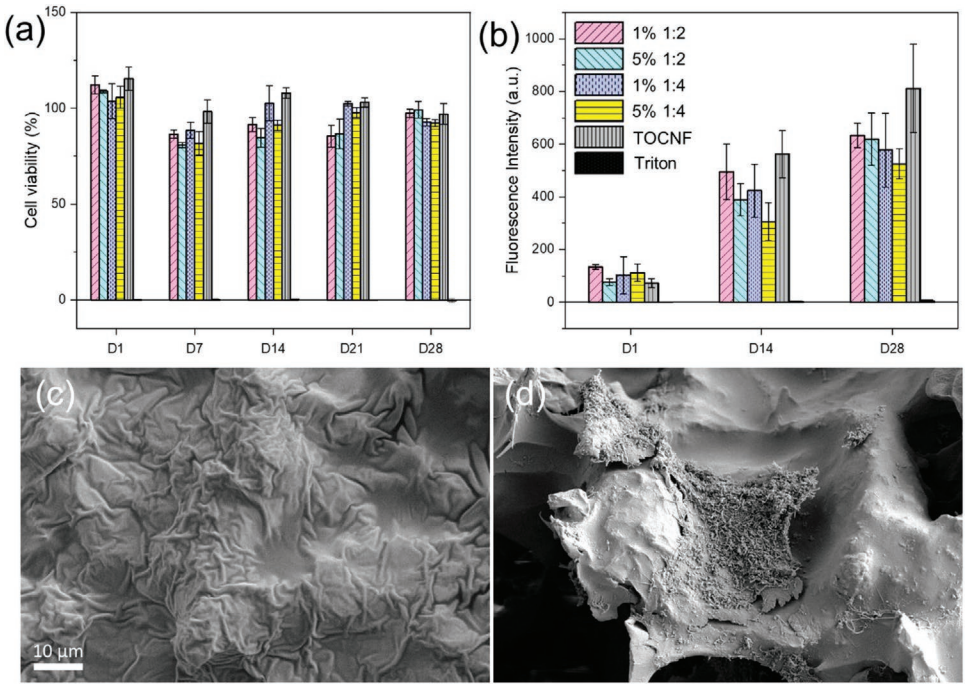

Figure 5. a) Cytotoxicity and b) H9c2 cardiomyoblast proliferation during 28 days analyzed by MTT and alamarBlue assays, respectively. Blank incubated medium was used as a positive control for cytotoxicity tests ($n = 4$). Cell attachment of c) control sample 5% 1:2 and d) 5% 1:2 sample, containing H9c2 cells. The magnification for (a) and (b) is 1000× .

2.2.6. Drug Release

The release profiles of the two model drugs tested were determined for composite patches following ink- and immersion-loading. The experiments included single drug delivery and codelivery in PBS physiological solution (pH 7.4) and MES buffer corresponding to the pH of typical infarcted heart tissue (pH 6).[67] Curcumin was used as an antioxidant and anti-inflammatory agent[68,69] while 3i-1000 is an inhibitor of GATA4-NKX2-5 interaction, and used for repair of myocardium after injuries.[52,70,71] The drug loading was calculated from the amount of residual drug in the system extracted in ethanol. The ink-loading approach did not produce a significant drug incorporation. For the other systems, the loading values were calculated on the basis of mass was 1.6–0.8% and 0.2% for 3i-1000 and curcumin, respectively. Both drugs are hydrophobic and bear negative surface charges at pH 7.4 and 6.[69] Our results indicate that for all tested media conditions, the cumulative released amount of curcumin and 3i-1000 was <2% and ≈12%, respectively (**Figure 6**). The low curcumin release is likely related to its degradation, especially at 37 °C and pH 7.4 (physiological pH).[68] In MES (corresponding to a lower pH = 6), the release of curcumin was still low, but higher compared to that determined at physiological pH. As expected, 3i-1000 was released more extensively from patches that were immersion-loaded (Figure S4a, Supporting Information). The release of the drug from the structure is likely related to the degradation of the PGS component, which depends on the conditions used for PGS synthesis, such as pressure and temperature.[72] The PGS-TOCNF-PPy patches show a slow release of the model drugs, which degraded by 8% after 21 days (Figure 6b).

3. Conclusion

In this study, drug-loaded 3D-printed conductive patches were fabricated for intended uses in cardiac conditions. Porous nanocellulose, elastic PGS, and conductive PPy were incorporated in biocomposites with no need for crosslinkers. The cardiac patches showed high biocompatibility with cardiomyoblasts and induced cell proliferation for 28 days. Cells attached on the microstructure followed the same shape and pattern as those of the microstructural support. The patches were loaded inside the pores, which mostly controls the release, and also inside the structure, which is subjected to the degradation of PGS. The slow degradation of the cardiac patches is expected to prevent burst release and make them suitable for long-term codelivery of drugs for therapies after myocardial infarction

4. Experimental Section

Materials: Preparation of TEMPO oxidized nanocellulose is explained in details in the Supporting Information. Glycerol 85% was purchased from Yliopiston Apteekki, Finland. Sebacic acid, Pressed pellets of polypyrrole and 4-(2-hydroxyethyl)-1-piperazineethanesulfonic acid (HEPES) were obtained from Sigma Aldrich and Hank's buffered salt solution (HBSS) 10× was obtained from Gibco Life Technologies. Curcumin was purchased from Chemcruz.

Design and Fabrication of Elastic and Conductive Patches—Ink Composition: Prepolyglycerol sebacate (pre-PGS) prepared as described in the previous work. Briefly, equimolar solutions of sebacic acid and glycerol (0.05 M) were mixed at 120 °C under argon gas for 24 h. Afterward, tip-sonicated PPy dispersion in tetrahydrofuran (THF) was added (1 or 5% w/v), and the mixture was stirred for 48 h at room temperature. TOCNF suspension was then mixed (IKA T-25 Ultra-Turrax)

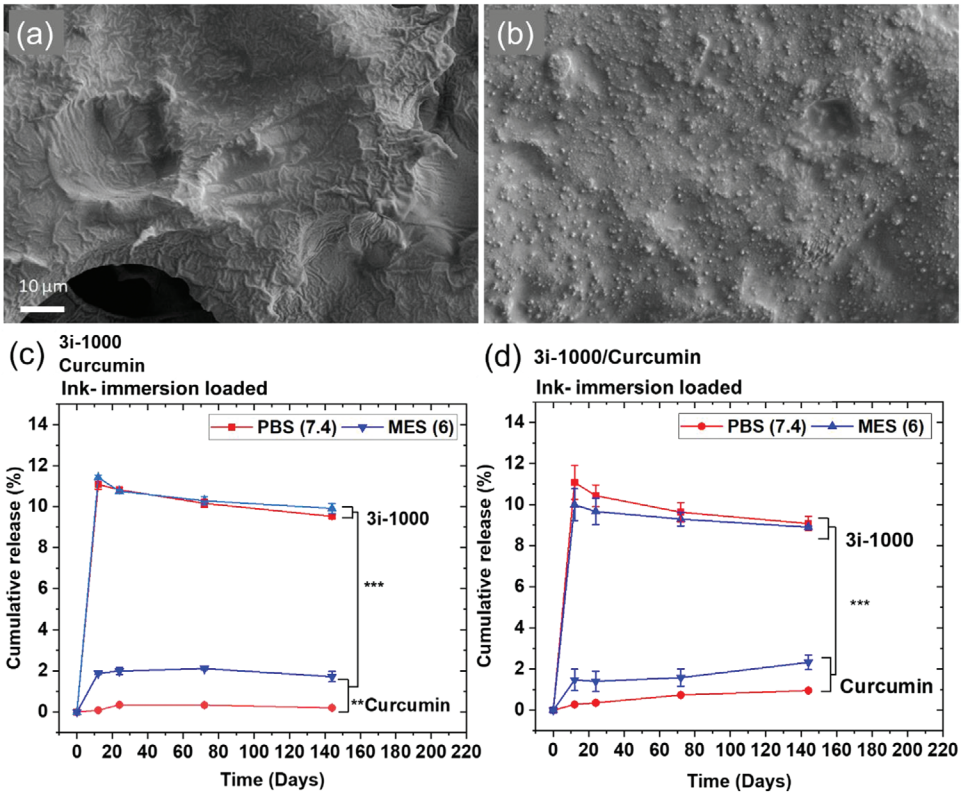

Figure 6. SEM images of the surface of a) drug-free and, b) drug-loaded biocomposites (1000× magnification, scale bar of 10 µm). Cumulative drug (3i-1000 and curcumin) release profiles from the porous biocomposites after ink-immersion loading using a c) single-drug or d) coloading (3i-100/curcumin) in PBS (pH 7.4, square symbols) and MES (pH 6, circle symbols). Statistical data were obtained by one-way analysis of variance (ANOVA) with a level of significance at probabilities of $^{**}p < 0.01$ and $^{***}p < 0.001$.

to obtain nanocellulose-based ink of varying ratios, 0:1 (pre-PGS-PPy: TOCNF), 1:2 and 1:4 (**Table 2**).

Design and Fabrication of Elastic and Conductive Patches—3D Printing of the Composite Ink: A BIO X Bioprinter (CELLINK, Gothenburg, Sweden) equipped with pneumatic print-head was used to print the cardiac patches. All samples were designed to be rectangular grid with a rectilinear infill pattern and 25% infill density. The system utilized clear pneumatic 3 mL syringes and sterile blunt needles, 18G from CELLINK, with the nozzle tip size of 0.84 mm. The solid support used for 3D printing consisted of plastic Petri dishes (100 mm diameter).

Printing parameters, including nozzle size, print speed, and extrusion pressure were adjusted to achieve suitable conditions for 3D printing of nanocellulose-based cardiac patches of high visual quality. After 3D printing, the samples were frozen overnight at –18 °C followed by freeze-drying with a FreeZone 2.5 L Benchtop Freeze Dryer for 48 h at –49 °C and 0.05 mbar to avoid extensive biocomposite shrinkage upon removal of water. Following, PGS synthesis from the prepolymer was achieved by curing the patches for 48 h in a vacuum oven at 120 °C.

Table 2. Ink composition in 3D printed cardiac patches.

Sample	PPy [w/v %]	Pre-PGS:TOCNF volume-to-weight ratio
TOCNF	0	0:1
1% 1:2	1	1:2
1% 1:4	1	1:4
5% 1:2	5	1:2
5% 1:4	5	1:4

Characterization of 3D Printed Patches—Transmission Electron Microscopy: TEM imaging of nanocellulose-based cardiac patches was performed with a JEM-2800 (JEOL) high-resolution TEM microscope operating at 200 kV. A small piece of porous nanocellulose-based structure was embedded in epoxy resin to form a block surrounding the sample. The block was trimmed in the shape of trapezoid to ease slicing in thin sections. An Ultramicrotome Leica UC7 with a Diatome Cryo Wet 35 diamond knife was used to cut 3D printed cured samples of 50 nm thickness. The serial sections were separated by an eyelash brush and directly collected from the surface of water by using an iron ring on the TEM grid.

Characterization of 3D Printed Patches—Microstructure: The microstructure of extruded patches after freeze drying was observed by SEM (Zeiss Sigma VP, Germany and Hitachi S-4800, Japan) operated under vacuum and at an accelerated voltage of 5–10 kV. To examine the microstructure in the absence of TOCNF, the PGS-PPy 5% was casted in glass Petri dishes and cured for 48 h at 120 °C. The dry samples were fixed on metal stubs using carbon tape and coated with a 4–5 nm layer of gold palladium alloy using a LEICA EM ACE600 sputter coater.

Characterization of 3D Printed Patches—Porosity: Ethanol replacement method was used to evaluate the porosity of 3D printed samples.[18,73] In this method, dry 3D printed cubes (1 cm × 1 cm × 1 cm) were immersed in excess pure ethanol for 48 h. The weight change was monitored until constant weight. The porosity Φ was then calculated following Equation (1), where m_{sat} is the weight of the sample saturated with ethanol, m_d is the dry mass, ρ is the density of ethanol, and V is the apparent volume. The reported values are the average of three replicates

$$\Phi(\%) = \left(\frac{(m_{sat} - m_d)/\rho}{V} \right) \times 100 \quad (1)$$

Characterization of 3D Printed Patches—Mechanical Properties: Samples were 3D printed with 100% infill and gauge length of 50 mm according to ASTM A370 standard. The tensile properties were tested with a Universal Instron 4240 testing machine using 100 N load. The test speed was 3 mm min^{-1}, and the gauge length was 30 mm. Before any tests, the 3D-printed samples were equilibrated for 24 h in a room kept at constant temperature (23 °C) and 50% humidity.

Characterization of 3D Printed Patches—Conductivity: A four-point probe test unit (Jandel Model RM3000), which combined a constant current source and a digital voltmeter, was used to measure the sheet resistance of the cardiac patches. 3D-printed grid lattice structures with 25% infill and 1 mm thickness were used for the conductivity measurements. The conductivity was calculated using Equation (2), where R corresponds to Ohms $square^{-1}$ and t is sample thickness in cm. A caliper was used to measure the thickness of each sample. The reported values are the average of 10 measurements on different spots of the sample[17]

$$\text{Conductivity}\left(\text{Scm}^{-1}\right) = \frac{1}{R \times t} \tag{2}$$

Characterization of 3D Printed Patches—Degradation and Swelling of 3D printed Scaffolds: For degradation and swelling studies of the conductive patches, samples were cut with the same sizes and weighted (W_0) (four replicates). They were immersed in 3 mL buffer solutions, MES (pH 6), and PBS (pH 7.4) for 21 days at 37 °C. At each time point, samples were taken from the buffer, and the excess water on the surface was wiped with filter paper and weighted in the wet state (W_s). The pH of the samples was checked for each buffer. The samples were dried at 37 °C for 24 h and weighted again in the dry state (W_d). The % swelling and biodegradation was calculated by using Equations (3) and (4), respectively

$$\text{Swelling}\,\% = \frac{(W_s - W_0)}{W_0} \times 100 \tag{3}$$

$$\text{Biodegradation}\,\% = \frac{(W_0 - W_d)}{W_0} \times 100 \tag{4}$$

Characterization of 3D Printed Patches—Cell Viability, Proliferation, and Attachment: The cardiomyoblast–biocomposite interactions were studied following our previous works explained in the Supporting Information.[3,17] Also, cell attachment on the 3D-printed 5% 1:2 patch was studied by SEM during 4 days. First, samples were sterilized by UV light for 3 h and trapped in the bottom of the 48-well plates by Pyrex cylinders and immersed inside Dulbecco's Modified Eagle's Medium with 10% of fetal bovine serum, with 1% (w/v) L-glutamine, 1% (w/v) non-essential amino acids, and penicillin-streptomycin (100 IU mL^{-1}) for 24 h before 20 000 H9c2 cells were seeded on top of each sample. At each time point, each sample was washed twice with PBS (pH 7.4), and attached cells were fixed with 2.5% glutaraldehyde in PBS at 37 °C for 30 min, and then washed gently with PBS (pH 7.4) three times before post-fixation with 1% of osmium tetroxide in PBS for 1 h. Samples were dehydrated using 50%, 70%, 96%, and 100% of EtOH and dried by critical point drying method and later coated with a 4 nm layer of gold palladium alloy using a LECIA EM ACE600 sputter coater and imaged by SEM (Zeiss Sigma VP, Germany) operated under vacuum and at an accelerated voltage of 5 kV.

Drug Loading and Release: Pre-PGS was prepared by polycondensation of equimolar mixtures of sebacic acid and glycerol at 120 °C in neutral condition for 24 h. The prepolymer was dissolved in THF and 5% w/v PPy were tip sonicated and added to the mixture. The suspension was stirred for 48 h in room temperature before adding TOCNF yielding pre-PGS-PPy:TOCNF (1:2) in a glass bottle. This suspension (ink) was homogenized and divided into two different series to produce the respective patches, with and without drug. They were transferred into large syringes and loaded with 3i-1000 (2 mg mL^{-1}), curcumin (2 mg mL^{-1}), and the 3i-1000/curcumin (1:1) mixture (coloading) (2 mg mL^{-1}) all in ethanol. Syringes were kept on a shaker for 2 h at room temperature. The ink samples (drug-loaded or drug-free) were transferred into clear pneumatic 3 mL syringes, and cylinders were printed with 100% infill of grid lattice pattern (patches); a needle size of 0.84 mm was used in the bioprinter (ink loaded samples). Samples were immediately frozen and freeze-dried at –49 °C for 48 h. The two types of 3D-printed patches were cured in a vacuum oven for 48 h at 120 °C.

Patches that were subjected to immersion-loading (Figure S5a, Supporting Information) and combination of immersion-loading and ink-loading (Figure S5b, Supporting Information) were immersed in drug solutions in EtOH (2 mg mL^{-1}) for 2 h in a shaker operated at 600 rpm and washed once with MQ-water. Following, the samples were immersed in 10 mL of MES medium (pH 6) and PBS (pH 7.4). At given time periods, 1 mL of each media was replaced by fresh medium (to maintain a constant volume). Drug release was analyzed for five months by using high-performance liquid chromatography (HPLC) (Agilent 1260, Agilent Technologies, USA) with a LC column (100 × 4.6 mm, 3 µm, Gemini NX-C18, Phenomenex, Denmark), using a mobile phase comprising 0.1% of phosphoric acid (PA):acetonitrile (ACN) (75:25 v/v), a flow rate of 1 mL min^{-1} and injection volume of 20 µL. The column operated at 25 °C and detection wavelength of 280 nm. For calculating the drug release, the total area under the peaks for 3i-1000 and curcumin were used after each measurement.

Characterization of 3D Printed Patches—Statistical Analyses: The results were reported as mean ± standard deviations (S.D.) of three to four independent sets of measurements. Statistical analysis was based on a one-way analysis of variance (ANOVA) with a level of significance set at probabilities of $*p < 0.05$, $**p < 0.01$, $***p < 0.001$, examined with OriginPro8.6 software.

Supporting Information

Supporting Information is available from the Wiley Online Library or from the author.

Acknowledgements

R.A. and N.Z.E. contributed equally to this work. O.J.R. acknowledges funding from the European Research Council (ERC) under the European Union's Horizon 2020 research and innovation programme (ERC Advanced Grant Agreement No. 788489, "BioElCell") and the funding support by the Academy of Finland's Biofuture 2025 program under project 2228357-4 (3D Manufacturing of Novel Biomaterials). H.A.S. acknowledges financial support from the HiLIFE Research Funds, the Sigrid Jusélius Foundation, and the Academy of Finland (decision no. 317042). H.R. acknowledges funding from Business Finland (3iRegeneration, project 40395/13), the Finnish Foundation for Cardiovascular Research, and the Sigrid Jusélius Foundation. R.A acknowledges funding from Finnish Foundation for Technology Promotion (TES). The authors thank the Electron Microscopy Unit of the Institute of Biotechnology, University of Helsinki and Aalto University's Nanomicroscopy Center, for providing laboratory facilities and assistance.

Conflict of Interest

The authors declare no conflict of interest.

Keywords

cardiac myoblasts, cardiac patches, direct ink writing, drug release, nanocellulose

Received: April 19, 2020
Published online:

[1] L. Bacakova, J. Pajorova, M. Bacakova, A. Skogberg, P. Kallio, K. Kolarova, V. Svorcik, *Nanomaterials* **2019**, *9*, 164.
[2] R. Curvello, V. S. Raghuwanshi, G. Garnier, *Adv. Colloid Interface Sci.* **2019**, *267*, 47.
[3] R. Ajdary, S. Huan, N. Zanjanizadeh Ezazi, W. Xiang, R. Grande, H. A. Santos, O. J. Rojas, *Biomacromolecules* **2019**, *20*, 2770.
[4] C. Xu, B. Zhang Molino, X. Wang, F. Cheng, W. Xu, P. Molino, M. Bacher, D. Su, T. Rosenau, S. Willför, G. Wallace, *J. Mater. Chem. B* **2018**, *6*, 7066.
[5] S. Derakhshanfar, R. Mbeleck, K. Xu, X. Zhang, W. Zhong, M. Xing, *Bioact. Mater.* **2018**, *3*, 144.
[6] X. Xu, J. Zhou, Y. Jiang, Q. Zhang, H. Shi, D. Liu, *J. Biomater. Sci., Polym. Ed.* **2018**, *29*, 1498.
[7] J. Liu, F. Cheng, H. Grénman, S. Spoljaric, J. Seppälä, J. E. Eriksson, S. Willför, C. Xu, *Carbohydr. Polym.* **2016**, *148*, 259.
[8] F. V. Ferreira, L. P. Souza, T. M. M. Martins, J. H. Lopes, B. D. Mattos, M. Mariano, I. F. Pinheiro, T. M. Valverde, S. Livi, J. A. Camilli, A. M. Goes, R. F. Gouveia, L. M. F. Lona, O. J. Rojas, *Nanoscale* **2019**, *11*, 19842.
[9] R. Poonguzhali, S. Khaleel Basha, V. Sugantha Kumari, *Polym. Bull.* **2018**, *75*, 4165.
[10] K. Rodríguez, P. Gatenholm, S. Renneckar, *Cellulose* **2012**, *19*, 1583.
[11] I. Buj-Corral, A. Bagheri, O. Petit-Rojo, *Materials* **2018**, *11*, 1532.
[12] S. Sultan, A. P. Mathew, *Nanoscale* **2018**, *10*, 4421.
[13] K. M. O. Håkansson, I. C. Henriksson, C. de la Peña Vázquez, V. Kuzmenko, K. Markstedt, P. Enoksson, P. Gatenholm, *Adv. Mater. Technol.* **2016**, *1*, 1600096.
[14] A. Saudi, M. Rafienia, A. Zargar Kharazi, H. Salehi, A. Zarrabi, M. Karevan, *Polym. Adv. Technol.* **2019**, *30*, 1427.
[15] R. Rai, M. Tallawi, A. Grigore, A. R. Boccaccini, *Prog. Polym. Sci.* **2012**, *37*, 1051.
[16] Y. Jia, W. Wang, X. Zhou, W. Nie, L. Chen, C. He, *Polym. Chem.* **2016**, *7*, 2553.
[17] N. Zanjanizadeh Ezazi, R. Ajdary, A. Correia, E. Mäkilä, J. Salonen, M. Kemell, J. Hirvonen, O. J. Rojas, H. J. Ruskoaho, H. A. Santos, *ACS Appl. Mater. Interfaces* **2020**, *12*, 6899.
[18] N. Zanjanizadeh Ezazi, M. A. Shahbazi, Y. V. Shatalin, E. Nadal, E. Mäkilä, J. Salonen, M. Kemell, A. Correia, J. Hirvonen, H. A. Santos, *Int. J. Pharm.* **2018**, *536*, 241.
[19] H. S. O'Neill, L. B. Gallagher, J. O'Sullivan, W. Whyte, C. Curley, E. Dolan, A. Hameed, J. O'Dwyer, C. Payne, D. O'Reilly, E. Ruiz-Hernandez, E. T. Roche, F. J. O'Brien, S. A. Cryan, H. Kelly, B. Murphy, G. P. Duffy, *Adv. Mater.* **2016**, *28*, 5648.
[20] Z. B. Huang, G. F. Yin, X. M. Liao, J. W. Gu, *Front. Mater. Sci.* **2014**, *8*, 39.
[21] D. D. Ateh, H. A. Navsaria, P. Vadgama, *J. R. Soc., Interface* **2006**, *3*, 741.
[22] Cardiovascular diseases, https://www.who.int/health-topics/cardiovascular-diseases/#tab=tab_1 (accessed: April 2020).
[23] V. Talman, H. Ruskoaho, *Cell Tissue Res.* **2016**, *365*, 563.
[24] S. Dimmeler, J. Burchfield, A. M. Zeiher, *Arterioscler., Thromb., Vasc. Biol.* **2008**, *28*, 208.
[25] K. Malliaras, E. Marbán, *Br. Med. Bull.* **2011**, *98*, 161.
[26] M. T. Alrefai, D. Murali, A. Paul, K. M. Ridwan, J. M. Connell, D. Shum-Tim, *Stem Cells Cloning Adv. Appl.* **2015**, *8*, 81.
[27] S. L. White, R. Hirth, B. Mahíllo, B. Domínguez-Gil, F. L. Delmonico, L. Noel, J. Chapman, R. Matesanz, M. Carmona, M. Alvarez, J. R. Nunez, A. Leichtman, *Bull W. H. O.* **2014**, *92*, 826.
[28] M. Domenech, L. Polo-Corrales, J. E. Ramirez-Vick, D. O. Freytes, *Tissue Eng., Part B* **2016**, *22*, 438.
[29] Q. L. Wang, H. J. Wang, Z. H. Li, Y. L. Wang, X. P. Wu, Y. Z. Tan, *J. Cell. Mol. Med.* **2017**, *21*, 1751.
[30] J. A. Sanz-Herrera, E. Reina-Romo, *Int. J. Mol. Sci.* **2011**, *12*, 8217.
[31] N. Noor, A. Shapira, R. Edri, I. Gal, L. Wertheim, T. Dvir, *Adv. Sci.* **2019**, *6*, 1900344.
[32] M. Qasim, F. Haq, M. H. Kang, J. H. Kim, *Int. J. Nanomed.* **2019**, *14*, 1311.
[33] J. Zhou, J. Chen, H. Sun, X. Qiu, Y. Mou, Z. Liu, Y. Zhao, X. Li, Y. Han, C. Duan, T. Tang, C. Wang, W. Zhong, J. Liu, Y. Luo, X. M. Mengqiu, C. Wang, *Sci. Rep.* **2014**, *4*, 3733.
[34] D. Bejleri, B. W. Streeter, A. L. Y. Nachlas, M. E. Brown, R. Gaetani, K. L. Christman, M. E. Davis, *Adv. Healthcare Mater.* **2018**, *7*, 1800672.
[35] H. S. O'Neill, J. O'Sullivan, N. Porteous, E. Ruiz-Hernandez, H. M. Kelly, F. J. O'Brien, G. P. Duffy, *J. Tissue Eng. Regener. Med.* **2018**, *12*, e384.
[36] T. Dvir, B. P. Timko, M. D. Brigham, S. R. Naik, S. S. Karajanagi, O. Levy, H. Jin, K. K. Parker, R. Langer, D. S. Kohane, *Nat. Nanotechnol.* **2011**, *6*, 720.
[37] N. Lang, E. Merkel, F. Fuchs, D. Schumann, D. Klemm, F. Kramer, S. Mayer-Wagner, C. Schroeder, F. Freudenthal, H. Netz, R. Kozlik-Feldmann, M. Sigler, *Eur. J. Cardio-Thoracic Surg.* **2015**, *47*, 1013.
[38] D. Zhang, I. Y. Shadrin, J. Lam, H. Q. Xian, H. R. Snodgrass, N. Bursac, *Biomaterials* **2013**, *34*, 5813.
[39] M. Boffito, S. Sartori, C. Mattu, G. Ciardelli, *Polyurethanes for Cardiac Applications*, Elsevier Ltd, Amsterdam **2016**.
[40] S. Asadpour, H. Yeganeh, J. Ai, S. Kargozar, M. Rashtbar, A. Seifalian, H. Ghanbari, *ACS Biomater. Sci. Eng.* **2018**, *4*, 4299.
[41] Y. Liu, S. Wang, R. Zhang, *Int. J. Biol. Macromol.* **2017**, *103*, 1130.
[42] Y. Chen, J. Wang, B. Shen, C. W. Y. Chan, C. Wang, Y. Zhao, H. N. Chan, Q. Tian, Y. Chen, C. Yao, I.-. M. Hsing, R. A. Li, H. Wu, *Macromol. Biosci.* **2015**, *15*, 426.
[43] H.-L. Tan, S.-Y. Teow, J. Pushpamalar, *Bioengineering* **2019**, *6*, 17.
[44] R. Ravichandran, R. Sridhar, J. R. Venugopal, S. Sundarrajan, S. Mukherjee, S. Ramakrishna, *Macromol. Biosci.* **2014**, *14*, 515.
[45] N. Reddy, R. Reddy, Q. Jiang, *Trends Biotechnol.*. **2015**, *33*, 362.
[46] P. Siqueira, É. Siqueira, A. E. de Lima, G. Siqueira, A. D. Pinzón-Garcia, A. P. Lopes, M. E. C. Segura, A. Isaac, F. V. Pereira, V. R. Botaro, *Nanomaterials* **2019**, *9*, 78.
[47] D. Kilian, T. Ahlfeld, A. R. Akkineni, A. Lode, M. Gelinsky, *MRS Bull.*. **2017**, *42*, 585.
[48] G. Yang, Z. Xiao, H. Long, K. Ma, J. Zhang, X. Ren, J. Zhang, *Sci. Rep.* **2018**, *8*, 1.
[49] D. Lelli, A. Sahebkar, T. P. Johnston, C. Pedone, *Pharmacol. Res.* **2017**, *115*, 133.
[50] M. Rahnavard, M. Hassanpour, M. Ahmadi, M. Heidarzadeh, H. Amini, M. Z. Javanmard, M. Nouri, R. Rahbarghazi, N. Safaie, *J. Cell. Biochem.* **2019**, *120*, 11965.
[51] M. P. A. Ferreira, S. Ranjan, S. Kinnunen, A. Correia, V. Talman, E. Mäkilä, B. Barrios-Lopez, M. Kemell, V. Balasubramanian, J. Salonen, J. Hirvonen, H. Ruskoaho, A. J. Airaksinen, H. A. Santos, *Small* **2017**, *13*, 1701276.
[52] S. M. Kinnunen, M. Tölli, M. J. Välimäki, E. Gao, Z. Szabo, J. Rysä, M. P. A. Ferreira, P. Ohukainen, R. Serpi, A. Correia, E. MÃ¤kilÃ, J. Salonen, J. Hirvonen, H. A. Santos, H. Ruskoaho, *Sci. Rep.* **2018**, *8*, 4611.
[53] S. T. Karhu, S. M. Kinnunen, M. Tölli, M. J. Välimäki, Z. Szabó, V. Talman, H. Ruskoaho, *Arch. Toxicol.* **2020**, https://doi.org/10.1007/s00204-020-02711-8.
[54] M. N. Hirt, A. Hansen, T. Eschenhagen, *Circ. Res.* **2014**, *114*, 354.
[55] R. Grande, E. Trovatti, A. J. F. Carvalho, A. Gandini, *J. Mater. Chem. A* **2017**, *5*, 13098.
[56] H. Meng, Q. Shi, T. Liu, F. X. Liu, P. Chen, *Energies* **2019**, *12*, 1.
[57] Z. Shi, H. Gao, J. Feng, B. Ding, X. Cao, S. Kuga, Y. Wang, L. Zhang, J. Cai, *Angew. Chem., Int. Ed.* **2014**, *53*, 5380.
[58] G. Nyström, A. Mihranyan, A. Razaq, T. Lindström, L. Nyholm, M. Strømme, *J. Phys. Chem. B* **2010**, *114*, 4178.
[59] M. Luo, M. Li, Y. Li, K. Chang, K. Liu, Q. Liu, Y. Wang, Z. Lu, X. Liu, D. Wang, *Compos. Commun.* **2017**, *6*, 68.
[60] Q. Chen, S. Liang, G. A. Thouas, *Prog. Polym. Sci.* **2013**, *38*, 584.

[61] T. H. Qazi, R. Rai, D. Dippold, J. E. Roether, D. W. Schubert, E. Rosellini, N. Barbani, A. R. Boccaccini, *Acta Biomater.* **2014**, *10*, 2434.
[62] M. J. Kim, M. Y. Hwang, J. Kim, D. J. Chung, *Biomed. Res. Int.* **2014**, *2014*, 1.
[63] Y. Xu, C. S. Kim, D. M. Saylor, D. Koo, *J. Biomed. Mater. Res., Part B* **2017**, *105*, 1692.
[64] N. Lin, A. Dufresne, *Eur. Polym. J.* **2014**, *59*, 302.
[65] J. Łojewska, P. Miśkowiec, T. Łojewski, L. M. Proniewicz, *Polym. Degrad. Stab.* **2005**, *88*, 512.
[66] S. Pashneh-Tala, R. Owen, H. Bahmaee, S. Rekštyte, M. Malinauskas, F. Claeyssens, *Front. Phys.* **2018**, *6*, 41.
[67] Z. Li, Z. Fan, Y. Xu, W. Lo, X. Wang, H. Niu, X. Li, X. Xie, M. Khan, J. Guan, *ACS Appl. Mater. Interfaces* **2016**, *8*, 10752.
[68] W.-H. Lee, C.-Y. Loo, M. Bebawy, F. Luk, R. Mason, R. Rohanizadeh, *Curr. Neuropharmacol.* **2013**, *11*, 338.
[69] M. Kharat, Z. Du, G. Zhang, D. J. McClements, *J. Agric. Food Chem.* **2017**, *65*, 1525.
[70] M. J. Välimäki, M. A. Tölli, S. M. Kinnunen, J. Aro, R. Serpi, L. Pohjolainen, V. Talman, A. Poso, H. J. Ruskoaho, *J. Med. Chem.* **2017**, *60*, 7781.
[71] S. T. Karhu, M. J. Välimäki, M. Jumppanen, S. M. Kinnunen, L. Pohjolainen, R. S. Leigh, S. Auno, G. Földes, G. Boije af Gennäs, J. Yli-Kauhaluoma, H. Ruskoaho, V. Talman, *Arch. Toxicol.* **2018**, *92*, 2897.
[72] X. Li, A. T. L. Hong, N. Naskar, H. J. Chung, *Biomacromolecules* **2015**, *16*, 1525.
[73] A. Shahini, M. Yazdimamaghani, K. J. Walker, M. A. Eastman, H. Hatami-Marbini, B. J. Smith, J. L. Ricci, S. V. Madihally, D. Vashaee, L. Tayebi, *Int. J. Nanomed.* **2013**, *9*, 167.